An analytical model for the upper bound estimation of respiratory motion–induced dose uncertainty in spot-scanning proton beam therapy

Heng Li[a], Xiaodong Zhang, Yupeng Li, and Ronald X. Zhu
Department of Radiation Physics, The University of Texas MD Anderson Cancer Center, Houston, TX, USA

(Received 18 December 2018; revised 13 August 2019; accepted for publication 14 August 2019; published xx xxxx xxxx)

Purpose: We developed an analytical model of a spot-scanning beam delivery system to estimate the upper bound of respiratory motion–induced dose uncertainty for a given treatment plan.
Methods: The effective delivery time for each spot position in the treatment plan was calculated on the basis of the parameters of the delivery system. The upper bound of the dose uncertainty was then calculated as a function of the effective delivery time. Two-dimensional (2D) measurements with a detector array on a one-dimensional moving platform were obtained to validate the model.
Results: We performed 351 two-dimensional measurements on a moving platform for different delivery sequences of a single-layer uniform pattern and patient treatment field. The measured dose uncertainty was a strong function of the effective delivery time: The shortest effective delivery time resulted in a maximum absolute dose error of >90%, while the longest ones resulted in a maximum absolute dose error of 4.9% for a single layer and 9.7% for a patient field with heterogeneity. The relationship of the effective delivery time and the measured dose uncertainty followed the analytical formula.
Conclusions: With our analytical model, the upper bound of the dose uncertainty due to motion can be estimated in spot-scanning proton therapy without four-dimensional dynamic dose calculation.
 [https://doi.org/10.1002/mp.13811]

Key words: motion, proton therapy, spot scanning

1. INTRODUCTION

Intensity-modulated proton therapy (IMPT) can result in a lower dose to normal tissue than does intensity-modulated photon radiotherapy (IMRT)[1] and has been implemented clinically for selected patients with lung cancer at the University of Texas MD Anderson Cancer Center Proton Therapy Center (Houston, Texas) (PTC-H).[2] However, dose uncertainty due to respiratory motion remains a major concern in treating lung and liver cancer patients.[3–5] Respiratory motion–induced dose uncertainty, often referred to as the interplay effect, could lead to large dose error within the target. Lambert et al. demonstrated that for patients treated with scanning proton beams, respiratory motion could introduce a maximum error of >60%, resulting in 100% of the target receiving a dose error of >5%, and that using margins around the tumor cannot compensate for the effect.[6] Bert et al. found in a planning study on five lung tumor patients that, due to interplay, the target volume receiving at least 95% of the prescribed dose was on average (standard deviation) 71.0% (14.2%), and concluded that interplay of scanned particle beams and moving targets has severe impact on the resulting dose distributions.[7] Owing to the potentially large dose error, the interplay effect has been studied extensively. The magnitude of motion-induced dose uncertainty was found to be delivery system dependent and patient specific, and could vary as a function of parameters including spot size,[4,8,9] fractionation,[4,8,10] rescanning,[4,11,12] delivery time,[8] scanning direction,[4,6] and patient breathing magnitude.[9] Four-dimensional (4D) dynamic dose, in which the delivered dose is calculated with consideration of time-dependent delivery sequence or radiation fluence along with patient anatomy under the influence of motion, has often been used to evaluate the interplay effect.[13] In essence, the spots in the treatment plan were first distributed to individual 4D computed tomography (4DCT) phases according to the timing of the delivery of each spot, which was calculated on the basis of spot delivery sequence and machine delivery parameters. The doses on different phases were then calculated using individual phase CTs and the assigned spot distribution. Finally, the individual phase doses were mapped to a reference phase using deformable image registration and accumulated as the 4D dynamic dose for a single delivery.[8,9,12,14–16] However, each pass of the 4D dynamic dose calculation is only the simulation of a single fraction of proton beam delivery, and even with repeated calculations to simulate the fractionated delivery, the sample size of the simulation is very limited given the size of all possible scenarios where tens of thousands of spots are assigned to ten breathing phases. Therefore, it is difficult to rely on 4D dynamic dose calculation to make clinical decisions, and a method to determine patient-specific dose uncertainty is needed for safe treatment of lung cancer patients using scanning beam proton therapy.

In this study, we developed and validated an analytical model to calculate the upper bound of respiratory motion–induced dose uncertainty.

2. MATERIALS AND METHODS

2.A. Spot-scanning delivery system

The Probeat spot-scanning delivery system (Hitachi America, Ltd., Tarrytown, NY) used at PTC-H was described in

detail by Gillin et al.[17] and Li et al.[16] The Probeat system generates a proton beam using a synchrotron with 94 discrete energies ranging from 72.5 to 221.8 MeV (4.0–30.6 cm in water). Each spill of proton particles by the synchrotron lasted a maximum of 4.4, and 2.1 s was required between spills for the deceleration and acceleration of protons. The proton beam was then diverted by the scanning magnets in the delivery nozzle to create spots that deliver a certain proton fluence to the desired depth and location in the patient. In this study, proton spots were modeled using a single two-dimensional (2D) Gaussian distribution[18,19] and characterized by the standard deviation (σ) of the Gaussian distribution. The spot size increases with decreasing initial particle energy, and σ ranges between 5.57 and 14.91 mm in air (for 221.8 and 72.5 MeV, respectively). The proton fluence delivered by each spot was characterized using the spot monitor unit (MU), which ranges from 0.005 to 0.04 MU[17]; the delivery time for each spot was 1–10 ms depending on the spot MU, and an interval of 3 ms between consecutive spots was used for internal checks by the delivery system. Therefore, each spot in a patient treatment plan is defined by the proton energy (which in turn defines both the depth dose and spot size), spot position at the isocenter plane ($\vec{u}$), and spot MU. In cases where the required spot dose exceeded 0.04 MU, the treatment planning system (Eclipse, Varian Medical Systems, Palo Alto, CA) generated the final DICOM treatment plan using a post-processing method that included splitting each spot into multiple spots that satisfied the MU limits and arranging the spots in a raster scanning fashion [Fig. 1(c)].[20]

2.B. Modeling the spot-scanning proton treatment plan and delivery

A detailed dose model of the spot-scanning proton beam in a commercial system was described by Zhu et al.[19]; a simplified model was used in this study.

The proton fluence of each spot could be described using a 2D fluence map, and each treatment field is a collection of spots, and thus, the summation of proton fluence maps. Considering spot delivery sequence, for a given spot-scanning proton treatment plan, the fluence map for each spot can be denoted as $F\left(\vec{u},e,k\right)$, where F is the pencil beam fluence map for spot number k on 2D space $\vec{u}$ that is perpendicular to the beam axis with energy e, and the fluence map has the unit MU.

Assuming the center of the spot at $\vec{u}_k$ has fluence MU_k, modeling the spot as a single Gaussian with σ_e will result in a spot fluence map that can be written as

$$\boldsymbol{F}\left(\vec{\boldsymbol{u}},\boldsymbol{e},\boldsymbol{k}\right)=\mathbf{MU}_{\boldsymbol{k}}\cdot\mathbf{exp}\left(-\frac{\left(\vec{\boldsymbol{u}}-\vec{\boldsymbol{u}}_{\boldsymbol{k}}\right)^2}{2\boldsymbol{\sigma}_{\boldsymbol{e}}^2}\right). \tag{1}$$

Given the proton dose calculation algorithm M and three-dimensional (3D) patient data $V\left(\vec{x}\right)$ but without considering motion, the 3D patient dose can be written as

$$\boldsymbol{D}_{3\boldsymbol{D}}=\iint_{\vec{\boldsymbol{u}}}\sum_{\boldsymbol{k}=1}^{\boldsymbol{K}}\boldsymbol{M}\left(\boldsymbol{F}\left(\vec{\boldsymbol{u}},\boldsymbol{e},\boldsymbol{k}\right),\boldsymbol{V}\left(\vec{\boldsymbol{x}}\right)\right). \tag{2}$$

With knowledge of the delivery system,[16] the delivery time needed for spot k can be calculated as $t_k=\frac{F(k)}{0.04}*0.01$ s; the total delivery time (s) to deliver spots 1 through k can be written as

$$\boldsymbol{T}_{\boldsymbol{k}}=\sum_{\boldsymbol{j}=1}^{\boldsymbol{k}}(\boldsymbol{t}_{\boldsymbol{j}}+0.003)+2.1\cdot\left(\sum\nolimits_{\boldsymbol{j}}\boldsymbol{t}_{\boldsymbol{j}}/4.4+\boldsymbol{e}_{\boldsymbol{k}}\right), \tag{3}$$

where the second part is the acceleration and deceleration time (2.1 s) needed between the spills ($\sum_j \boldsymbol{t}_j/4.4$, each spill could last up to 4.4 s) and the energy change($\boldsymbol{e}_k$, each energy change also takes 2.1 s). Therefore, the fluence map for spot k, $F\left(\vec{u},e,k\right)$ can also be written as $F\left(\vec{u},e,T_k\right)$, with the delivery time under consideration. Assuming the delivery starts at time t_0, the delivered dose to the patient can be written as

$$\boldsymbol{D}=\iint_{\vec{\boldsymbol{u}}}\sum_{\boldsymbol{k}=1}^{\boldsymbol{K}}\boldsymbol{M}\left(\boldsymbol{F}\left(\vec{\boldsymbol{u}},\boldsymbol{e}_{\boldsymbol{L}},\boldsymbol{t}_0+\boldsymbol{T}_{\boldsymbol{k}}\right),\boldsymbol{V}\left(\vec{\boldsymbol{x}},\boldsymbol{t}_0+\boldsymbol{T}_{\boldsymbol{k}}\right)\right), \tag{4}$$

where $V\left(\vec{x},t\right)$ is the patient volume information at time t, which is usually unknown. The 4D dose is the expectation of the delivered dose, regardless of the delivery modality (e.g., photon or proton), given the beam delivery and patient breathing are independent to each other[21]; thus, the 4D dose of the treatment plan described above can be written as

$$\boldsymbol{D}_{4\boldsymbol{D}}=\iint_{\vec{\boldsymbol{u}}}\sum_{\boldsymbol{k}=1}^{\boldsymbol{K}}\sum_{\boldsymbol{n}=1}^{\boldsymbol{N}}\frac{1}{\boldsymbol{N}}\boldsymbol{M}(\boldsymbol{F}(\boldsymbol{k}),\boldsymbol{V}(\boldsymbol{n})), \tag{5}$$

where $V\left(\vec{x},n\right)$ is the patient data (i.e., 4DCT) for phase n and N is the total number of phases. Delivery time is not a factor in the 4D dose calculation. The motion-induced dose uncertainty for a certain delivery can then be quantified by comparing the delivered dose and the 4D dose:

$$\Delta\boldsymbol{D}=\boldsymbol{D}-\boldsymbol{D}_{4\boldsymbol{D}}=\iint_{\vec{\boldsymbol{u}}}\sum_{\boldsymbol{k}=1}^{\boldsymbol{K}}\left[\boldsymbol{M}\left(\boldsymbol{F}(\boldsymbol{t}_0+\boldsymbol{T}_{\boldsymbol{k}}),\boldsymbol{V}(\boldsymbol{t}_0+\boldsymbol{T}_{\boldsymbol{k}})-\sum_{\boldsymbol{n}=1}^{\boldsymbol{N}}\frac{1}{\boldsymbol{N}}\boldsymbol{M}(\boldsymbol{F}(\boldsymbol{k}),\boldsymbol{V}(\boldsymbol{n}))\right)\right]. \tag{6}$$

Therefore, as demonstrated by Eq. (6), (a) dose uncertainty is a function of the delivery sequence (i.e., which spot was delivered at what time), and (b) the effect of dose uncertainty can be evaluated on surface $\vec{u}$; if the dose uncertainties for all locations on the surface are minimized, the total dose uncertainty will be minimized as well. As shown in previous studies[16,21,22] and as illustrated above, the motion-induced dose uncertainty decreases with a decreasing effective dose rate.

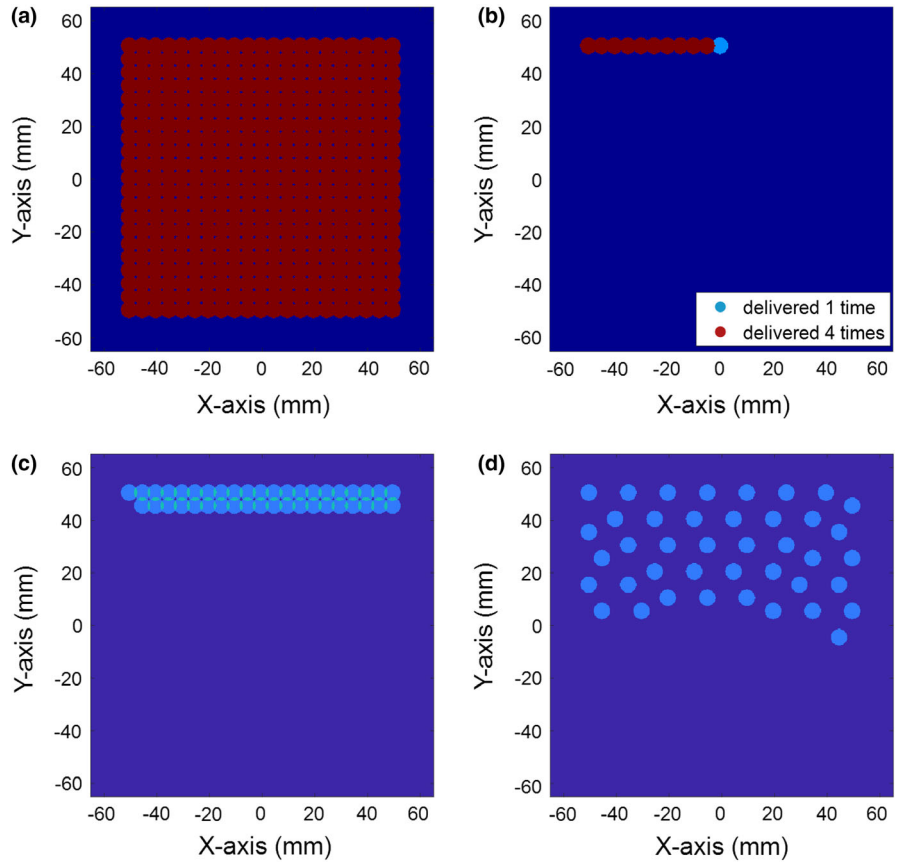

FIG. 1. Examples of different delivery sequences. (a) Spot pattern to be delivered. There were 1764 spots delivered to 441 spot positions (4 spots at each position), and the total delivery time was 15.5 s for all delivery sequences. Spots delivered within the first 0.5 s with the (b) worst delivery sequence, (c) raster scanning (with rescanning) deliver sequence, and (d) optimized delivery sequence are shown. Delivered spots are represented by a circle with a diameter of 5 mm for illustration purposes; spot spacing was 5 mm. Forty-one spots were delivered in 0.5 s. Color bar represents the number of rescanning, ranging from one to four.

2.C. Poisson model of motion-induced dose uncertainty for pulsed pencil beams

For a single pencil beam delivered in pulsed mode, the time difference between consecutive pencil beams can be modeled as a Poisson distribution, and the dose uncertainty becomes a function of the delivery time and breathing cycle[21]:

$$\triangle D = \triangle D^0_{\max} \frac{N}{2(N-1)} v^{-1} \mathrm{MAD}_{\mathrm{Poisson}}(v), \tag{7}$$

where $\triangle D^0_{\max}$ is the maximum possible dose error with 0 delivery time.

$$\mathrm{MAD}_{\mathrm{Poisson}}(v) = \frac{2\mathrm{e}^{-v} \cdot v^{\lfloor v \rfloor + 1}}{\lfloor v \rfloor !} \tag{8}$$

is the mean absolute deviation (MAD) of a Poisson distribution with parameter (mean) v; and $v = N\frac{T'_k}{T_b}$ is the effective number of deliveries per breathing phase (T_b/N, where T_b is the breathing period). Here, one could observe that assuming a fixed $\triangle D^0_{\max}$, dose uncertainty decreases with increasing v. In other words, dose uncertainty decreases when reducing the patient breathing period T_b, or increasing T'_k, the total effective delivery time (T') for spots 1 through k that contribute dose to the pencil beam location, as shown in the following equation:

$$\boldsymbol{T'}_k\left(\vec{\boldsymbol{u}}\right) = \boldsymbol{T'}_{k-1}\left(\vec{\boldsymbol{u}}\right) + \mathbf{min}\left(\boldsymbol{T}_k - \boldsymbol{T}\left(\vec{\boldsymbol{u}}\right), \frac{\boldsymbol{T}_b}{\boldsymbol{N}}\right) \frac{\boldsymbol{F}\left(\vec{\boldsymbol{u}}, \boldsymbol{e}, \boldsymbol{k}\right)}{\max\limits_{\boldsymbol{k}}\left(\boldsymbol{F}\left(\vec{\boldsymbol{u}}, \boldsymbol{e}, \boldsymbol{k}\right)\right)}. \tag{9}$$

$T\left(\vec{u}\right)$ denotes when the dose is delivered to position $\vec{u}$. $\min\left(T_k - T\left(\vec{u}\right), \frac{T_b}{N}\right)$ reflects that the time difference of successive delivery to the same spot could reduce the motion uncertainty, only up to T_b/N or the time length of a breathing phase, which is also the main difference between the delivery time and effective delivery time. For example, with a patient breathing period of 5 s, successive deliveries to the same spot position close to 0.5 s will be the most effective and efficient

in terms of reducing motion uncertainties, when considering motion mitigation techniques such as rescanning. This principle is also adopted in techniques such as phase-controlled scanning (PCR),[23–25] or breath sampling repainting.[11] Also note that T' is scaled by the spot fluence F.

2.D. Delivery time vs effective delivery time

T' differs from the delivery time because increasing the time between consecutive pencil beams is effective at reducing the dose uncertainty (up to T_b/N, after which there is no further benefit from increasing the time interval), as shown in our previous study.[21]

Figure 1(a) shows an example of a 10 × 10 cm uniform field of a single energy (173.7 MeV with a 20-cm range and σ = 6.75 mm). There were 441 spot positions with a spot spacing of 5 mm. We delivered 0.16 MU to each position in four spots of 0.04 MU each, and resulting in 1764 spots for the field. The total MU was 70.56, and the required time to deliver this field was 15.5 s. Figures 1(b) to 1(d) shows the first 0.5 s of delivery for three delivery schemes with the same overall delivery time (15.5 s) but very different effective delivery times for different spot positions: the worst spot delivery sequence with no rescanning (WS), where all MU to the same spot was delivered as quickly as possible, resulting in the minimized effective delivery time; the spot sequence with raster rescanning (RS), which has been adopted by commercial planning systems (e.g., Eclipse), where the spots were split according to the maximum MU constraint and delivered in a raster scanning fashion; and the optimized delivery sequence with spot repainting (OS) detailed in our previous study,[26] where the effective delivery time was maximized. Figure 1(c) shows the first 0.5 s of the RS plan as generated by the treatment planning system (Eclipse). The dose at any given spot position also contributes to nearby spot positions, depending on the spot size and spot spacing, as shown in Eq. (1). The spot delivery sequence in this case can be written as $\left(\vec{u}, T_k\right)$, and the first three spots can be written as (0 mm, 0 mm, 13 ms), (5 mm, 0 mm, 26 ms), and (10 mm, 0 mm, 39 ms). The corresponding pencil beam doses and timings delivered to (0 mm, 0 mm) can be written as (F, T_k): (0.04 MU, 13 ms), (0.03 MU, 26 ms), and (0.013 MU, 39 ms), where 0.03 and 0.013 MU are the fluences contributed by the second and third spots to location (0 mm, 0 mm), respectively. Figure 1(b) shows the WS plan, where the spot delivery sequence for the first three spots was (0 mm, 0 mm, 13 ms), (0 mm, 0 mm, 26 ms), and (0 mm, 0 mm, 39 ms), and the corresponding pencil beam doses and timings delivered to (0 mm, 0 mm) were (0.04 MU, 13 ms), (0.04 MU, 26 ms), and (0.04 MU, 39 ms). On the contrary, for the OS plan, with minimized dose uncertainty, the spots are placed far apart from each other so that the minimum dose is delivered to the same pencil beam location in any T_b/N interval [Fig. 1(d)]. The spot delivery sequence for the first three spots in this case was (0 mm, 0 mm, 13 ms), (15 mm, 0 mm, 26 ms), and (30 mm, 0 mm, 39 ms), and the corresponding pencil beam doses and timings delivered to (0 mm, 0 mm) were (0.04 MU, 13 ms), (0.003 MU, 26 ms), and (2×10^{-6} MU, 39 ms).

2.E. Maximum dose error as a function of motion range and spot size

In the formula for motion-induced dose uncertainty [Eq. (7)], the maximum possible dose error for a single delivery ($\triangle D^0_{\max}$) was used to normalize the dose uncertainty. Therefore, we quantitatively studied the factors that affect $\triangle D^0_{\max}$. There is a lack of studies of this topic specifically, but tumor motion is often modeled as powers of a sinusoidal function,[27,28] with motion amplitude A and period T_b. Using a single 2D Gaussian model of spot σ, we performed simple simulations to determine the relationship between $\triangle D^0_{\max}$, and A and σ.

A uniform field was generated (Fig. 2) by placement of spots with a size of σ = 6.75 mm at a spacing of d mm (d ranged from 1 to σ mm). With a one-dimensional motion range of 0–4 cm, the lower half of the spots was shifted upward, resulting in a dose error. The maximum dose error in this case could be derived as

$$\triangle D^0_{\max} = \mathrm{erf}\left(\frac{A}{2\sqrt{2}\sigma}\right), \tag{10}$$

where erf(x) is the error function. Simulations were performed as described below to confirm the result and showed that the maximum dose error increased with increasing motion range and decreasing spot size but not as a function of spot spacing, and the maximum dose error

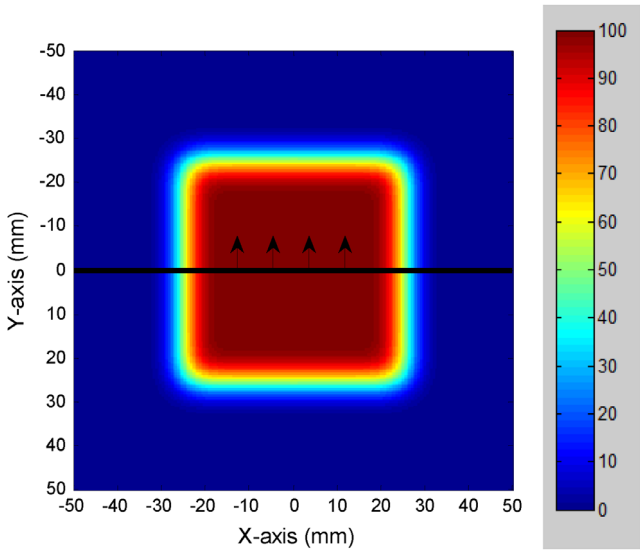

FIG. 2. The simulated proton fluence map of a uniform pattern with motion. The proton fluence map was generated using a single Gaussian model of spot size 6.75 mm and spot spacing of 2 mm. The upper half was stationary; the arrows indicate the motion of the lower half. Motion amplitude is 0 in the shown figure, and the color bar represents the percentage intensity of the proton fluence.

with this model was up to 100%. Measurement results were also compared with Eq. (10) to validate the calculation and simulation.

A similar relationship can also be established between $D^0_{\max}$ and water equivalent thickness change in the depth direction (△WET), with a known depth dose curve. However, since the dose falloff of the mono-energy proton beam Bragg peak in the depth direction is much steeper than the spot falloff in the lateral direction, we used $D^0_{\max} = 1$, that is, the maximum dose error of 100%, in this study for simplicity unless otherwise specified.

2.F. Dose error and energy layers

IMPT is usually delivered in a layer-by-layer fashion (i.e., all spots in a certain energy are delivered before the next proton energy starts). In the PTC-H system, the proton energies are delivered in a monotonically decreasing manner. As with the finite size of the proton spots, the proton spot dose is deposited not only to a certain depth but also along the beam path up to the depth determined by the proton energy. Therefore, for a certain beam angle, the higher energy layers contribute dose to voxels that are covered by lower energies and effectively reduce the dose rate to those voxels; the lower energies, on the other hand, do not contribute to deeper depth. As a result, qualitatively, the higher energy layers require more dose to each pencil beam location to deliver the same total dose to each voxel. That, along with a large spot size in the lower energy layers, indicates that spots and layers with lower energies require less splitting than do higher energies to achieve the same level of motion-induced dose uncertainty. A conservative estimate of the fluence contributed by a spot in a higher energy layer (e_H) to a lower energy layer (e_L) at pencil beam location $\vec{u}$ can be written as

$$F\left(\vec{u}, e_L, k\right) = F\left(\vec{u}, e_H, k\right) \frac{IDD_{e_H}\left(d_{\max}(e_L)\right)}{IDD_{e_L}\left(d_{\max}(e_L)\right)}, \tag{11}$$

where IDD is the integrated depth dose; e_H and e_L are the high and low energies, respectively; and $d_{\max}$ is the depth of the maximum dose (Bragg peak). Equation (11) is only exact at $d_{\max}(e_L)$; it underestimates the contribution from the high energy and is thus conservative.

2.G. Upper bound of dose error as a function of maximum dose error and effective delivery time

With the fluence map and delivery sequence for all energy layers established for a given treatment plan, the upper bound of the dose error of the treatment plan at all pencil beam positions can be estimated using Eqs. (7) to (9) and the following procedure:

1. Calculate the fluence at location $\vec{u}$ for pencil beam location $\vec{u}$,
2. for each energy, and
3. for each spot in this energy and all higher energies, calculate the fluence at location $\vec{u}$.
4. Calculate the total effective delivery time using Eq. (9).
5. Calculate the upper bound of the dose error from the 4D dose using Eq. (7).

2.H. Measurement setup

The measurement setup (Fig. 3) was described previously.[26]

A MatriXX multi-ion chamber detector (IBA Dosimetry, Schwarzenbruck, Germany) was placed on a 1D moving platform[29] and used to acquire the 2D dose distribution with and without motion. The MatriXX consists of 1020 vented pixel ionization chambers with 4.5 mm in diameter and 7.62 mm center to center spacing. While there could be dose averaging effect due to the finite size of the detector, we considered the ion chambers to be sufficiently small compared to the proton spot size (e.g., 173.7 MeV with a 20-cm range and σ = 6.75 mm). The 1D moving platform was driven by a VXM stepper motor controller attached to a BSlide assembly (Velmex, Inc., Bloomfield, NY). The motor controller can be programmed to move with different amplitudes and periods and can simulate most types of respiratory motion, including actual patient respiration.

2.I. Single-layer uniform pattern measurements

A single-layer, 10 × 10 cm uniform field [Fig. 1(a)] was delivered and measured using the setup shown in Fig. 3. We obtained 310 2D measurements using MatriXX, delivering the same total MU to each spot position under various motion conditions and spot

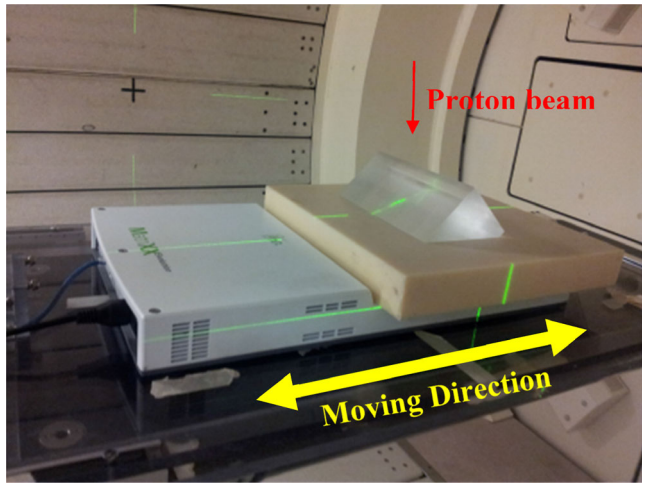

FIG. 3. Measurement setup using a 1D moving phantom with heterogeneity using a wedge with maximum △WET of 4.8 cm on a 5-cm-thick solid water slab

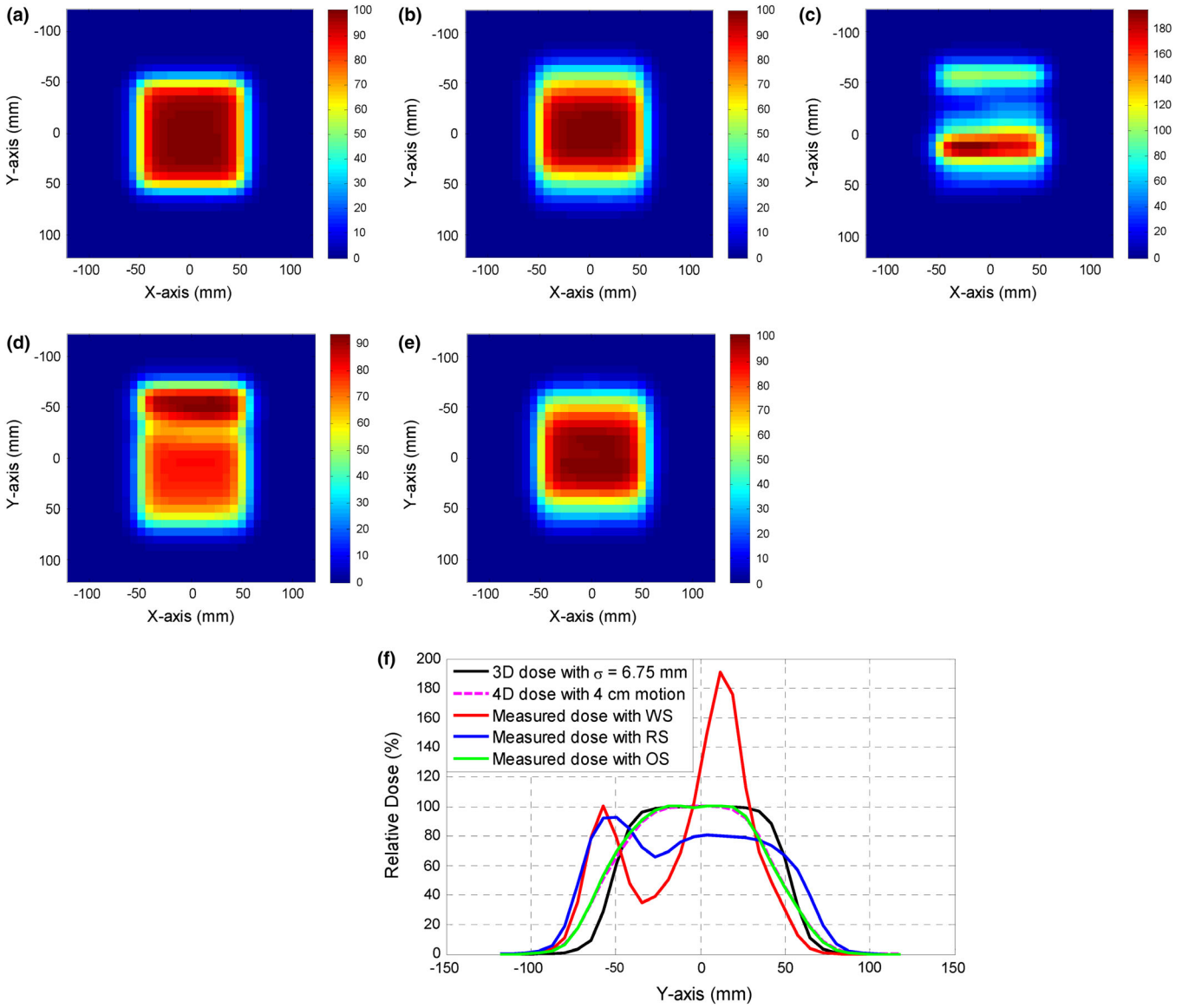

FIG. 4. (a) Nominal three-dimensional dose distribution for a single-layer uniform plan with $\sigma = 6.75$ mm and spot spacing of 5 mm. (b) Four-dimensional (4D) calculated dose distribution with 4-cm motion. (c) Single-fraction measured dose with the worst delivery sequence (maximum dose error up to 90%). (d) Raster scanning delivery sequence (maximum dose error up to 35%). (e) Optimized delivery sequence (maximum dose error 4.9%). (f) Plot of the y-axis with x = 0 for the nominal dose, 4D dose, and measured doses with worst (WS), optimized (OS), and raster (RS) scanning sequences. Color bar represents relative dose. Note that color scales are different for panels c and d to show the full range of dose.

delivery sequences. The following motion conditions were investigated:

1. Motion range (A): 0 to 4 cm
2. Motion period (T_b): 3 to 10 s
3. Motion pattern: $A\cos^{2n}\left(\frac{2\pi}{T_b}\cdot t\right)$, patient RPM pattern normalized to a given amplitude
4. Motion direction: parallel or perpendicular to scanning direction

First, we found that the motion pattern affects only the 4D dose calculation, not the maximum dose error between the measured dose and the 4D dose, that the motion direction perpendicular to the scanning direction yields the maximum dose error (data now shown), and that longer motion period results in larger dose error (When compare 3s period to 5s and 10s period, all with 1 cm range, the maximum dose error were 21%, 27% and 35%, respectively). Because of limited space, the results for these conditions were not presented separately. All results presented were measured under a motion direction perpendicular to the scanning direction with one motion pattern ($A\cos^4(\frac{2\pi}{T_b}t)$) unless otherwise specified.

For all motion conditions, the same spot pattern was delivered, with a spot size (σ) of 6.75 and 14.91 mm (173.7 MeV and 72.5 MeV).

We used the following delivery sequence:

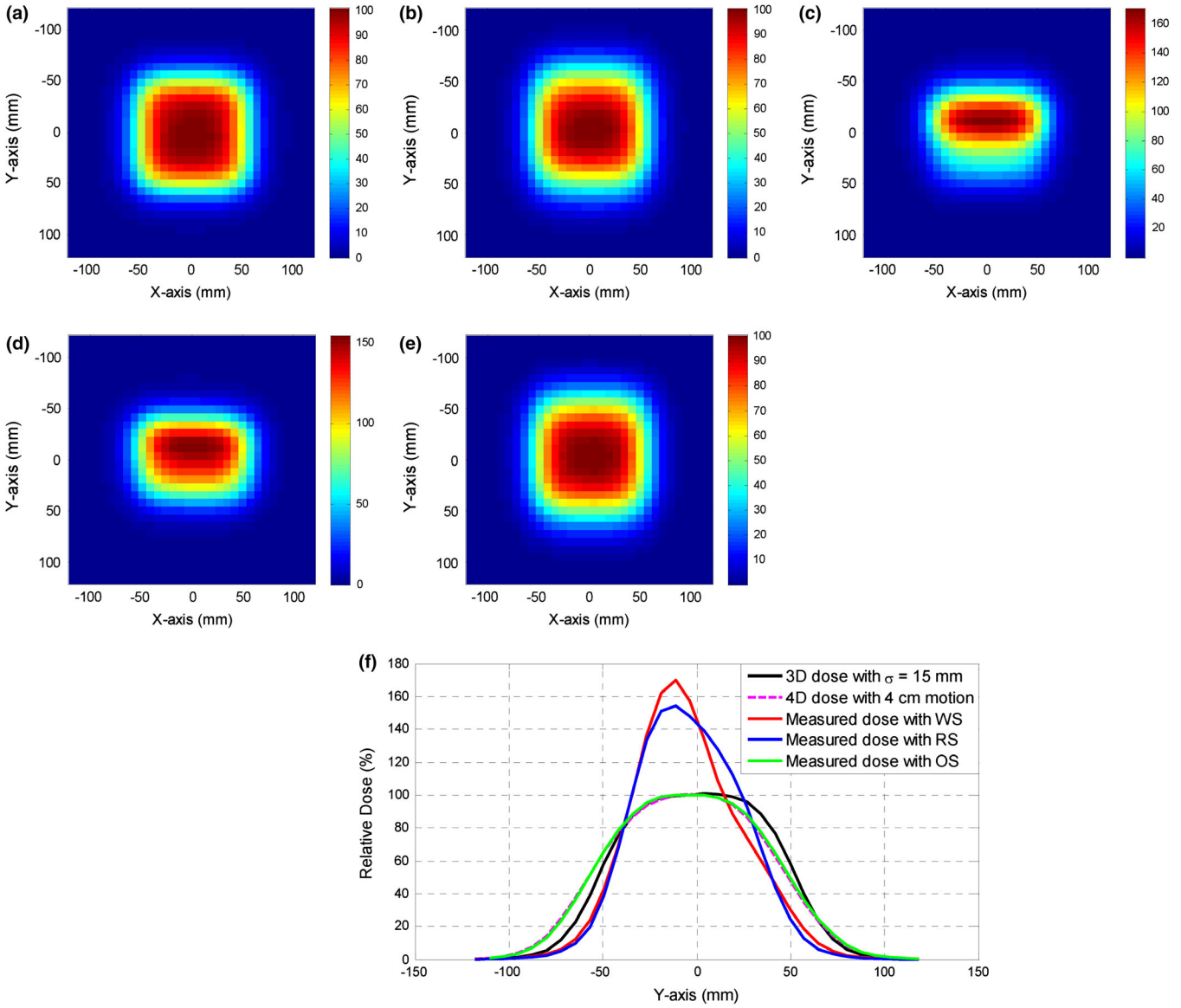

FIG. 5. (a) Nominal three-dimensional dose distribution for a single-layer uniform plan with σ = 15 mm and spot spacing of 5 mm. (b) Four-dimensional (4D) calculated dose distribution with 4-cm motion. (c) Single-fraction measured dose with worst delivery sequence (maximum dose error up to 65%), (d) for raster scanning delivery sequence (maximum dose error up to 50%), and (e) for optimized delivery sequence (maximum dose error 4.1%). (f) Plot of y-axis with x = 0 for nominal dose, 4D dose, and measured dose with worst (WS), optimized (OS), and raster (RS) scanning sequences. Color bar represents relative dose. Color scales are different for panels c and d.

1. Given 1, 2, 4, and 8 rescans, corresponding to delivery times of 16, 31, 42, and 84 s, respectively, the corresponding spot MUs were 0.04, 0.02, 0.01, and 0.005 per spot, respectively.
2. Given an optimized spot delivery sequence that corresponded to a delivery time of 55 s, the corresponding spot MUs varied with constraints of a maximum MU of 0.04 and a minimum MU of 0.005.

(1) and (2) resulted in five spot patterns with different numbers of spots and delivery times of 16, 31, 42, 84, and 55 s; the spot patterns were then formed into WS, RS, and OS delivery sequences for spot numbers in (1) and (2).

All spot sequences delivered the same amount of total MU; the central axis doses at the measurement plane were 138 cGy for spot size σ = 6.75 mm and 87 cGy for spot size σ = 14.91 mm.

2.J. Patient treatment plan measurements

A treatment plan for a patient with hepatic cancer was used for patient plan measurements. The treatment plan consisted of three fields for delivering 360 cGy (RBE) to CTV with single field optimization. For measurement purposes, one of the fields was renormalized to deliver all 360 cGy (RBE). The field size was about 12 × 12 cm, with 45 energy layers ranging from 155.3 to 86.4 MeV (proton range of 16.4

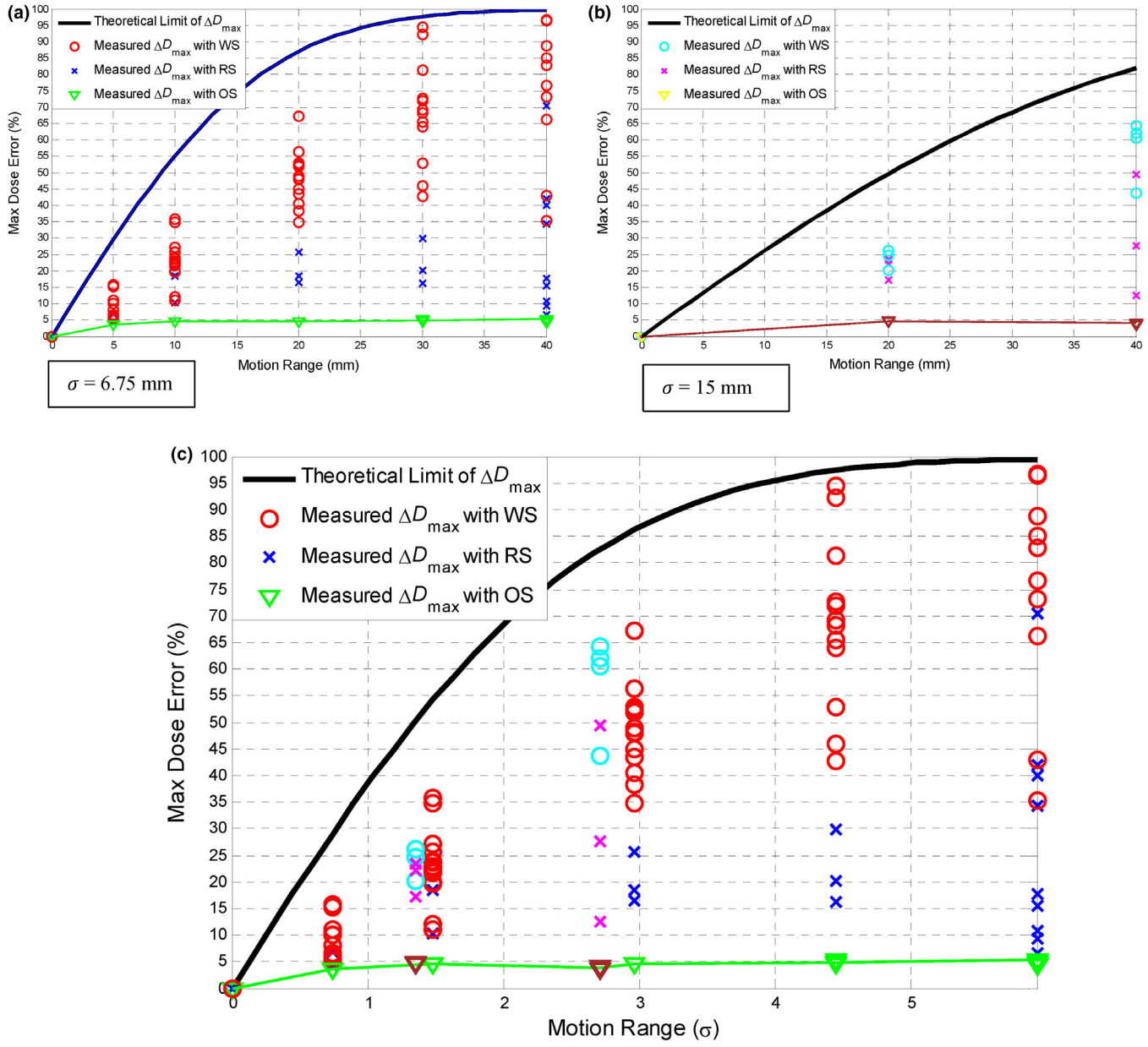

FIG. 6. Maximum dose error as a function of motion range and spot size. △Dmax as a function of motion range (a) in mm for a spot size of σ = 6.75 mm, (b) in mm for spot size of σ = 15 mm, and (c) in multiplication of σ for different delivery modes. In (c), different spot sizes are shown in different colors.

to 5.6 cm). The total delivery time for the original plan was 238 s. We developed an OS using the method described in the previous session; we considered all the delivery constraints and used criteria $T_k' \geq 30$ s, with a total delivery time of 357 s. WS, RS, and OS plans for each spot number (delivery time) were developed and delivered.

Thirty-six measurements were obtained with a 4-cm range, 10-s period, and 1D motion perpendicular to the scanning direction. To measure the dose error with heterogeneity, we placed an acrylic wedge on a 5-cm-thick solid water slab (Fig. 3). The cross section of the wedge was a right-angle triangle with a hypotenuse length of 13 cm. Therefore, the 4-cm motion range resulted in a maximum △WET of 4.8 cm.

3. RESULTS

3.A. Single-layer uniform pattern measurements

Figure 4 shows the results of measurement with 4 cm of motion for a single delivery of a single-layer 10 × 10 cm uniform field with σ = 6.75 mm. Figure 4(a) shows the measurement results with no motion. Figure 4(b) shows the calculated 4D dose based on the motion pattern, and Figs. 4(c) to 4(e) shows the measurement results for the RS, WS, and OS plans, respectively. Figure 4(f) shows the plot of the y-axis at x = 0 for the nominal, 4D, WS, OS, and RS plans in a single fraction. The maximum dose error between the delivered dose and the 4D dose was >90% for WS, >60% for RS, and 4.9% for OS.

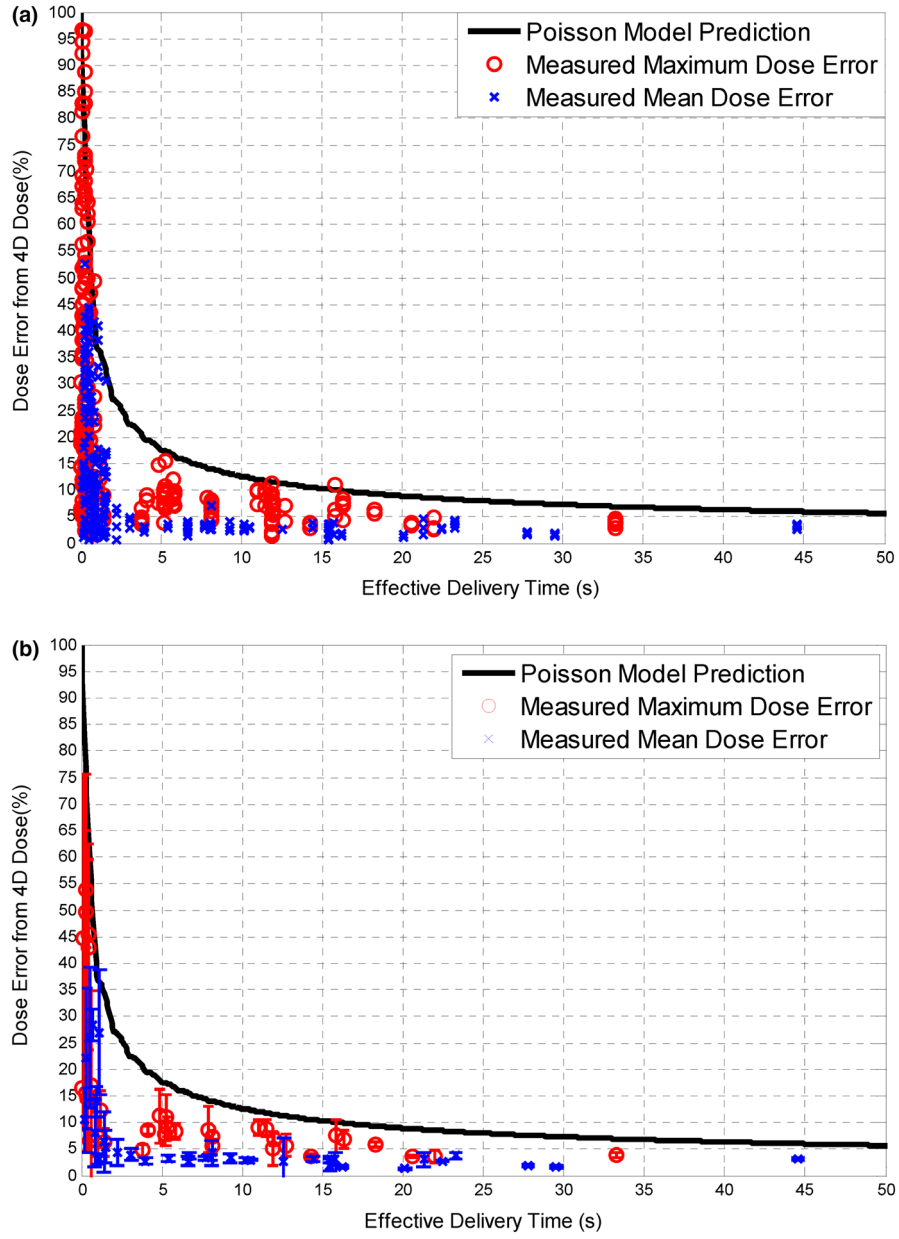

FIG. 7. Maximum and mean dose error as a function of the effective delivery time of the treatment plan (Poisson model estimation assumed △Dmax = 100%). (a) Maximum and mean dose errors of each measurement plot against the calculated minimum and mean effective delivery time for the corresponding treatment plan with a given delivery pattern. (b) Mean and standard deviations of the measured maximum and mean dose errors for a given effective delivery time.

Figure 5 shows the same measurements as in Fig. 4 but with a spot size of σ = 14.91 mm. The maximum dose error between the delivered dose and the 4D dose was >60% for WS, >50% for RS, and 4.1% for OS.

Figure 6 shows the relationship between the maximum dose error and the spot size. The simulation and calculation results of Eq. (10) matched perfectly (therefore only one line is visible), and both bounded the measurement results using WS, RS, or OS. Therefore, $\triangle D^0_{\max}$ could be calculated with known A and σ. However, in this study, we used a conservative number, $\triangle D^0_{\max}$ = 1, to avoid confusion. Also note that all measurements with OS, represented by the connected nabla symbol, are well below measurement for other two delivery sequences.

Figure 7 shows all 310 measurement results as a function of T'. For each delivery, T' of the center of each spot position was calculated, and the $T'_{\min}$ was plotted against the measured maximum absolute dose error between the measurement and the 4D dose $\triangle D_{\max}$. Similarly, the T'_{mean} was plotted against the mean absolute dose error between the measurement and the 4D dose $\triangle D_{\text{mean}}$. The theoretical upper bound of the dose error using the Poisson model in Eqs. (7) to (9) for a given T' was also plotted. Figure 7(a) shows individual measurement results, and Fig. 7(b) shows the mean and two standard

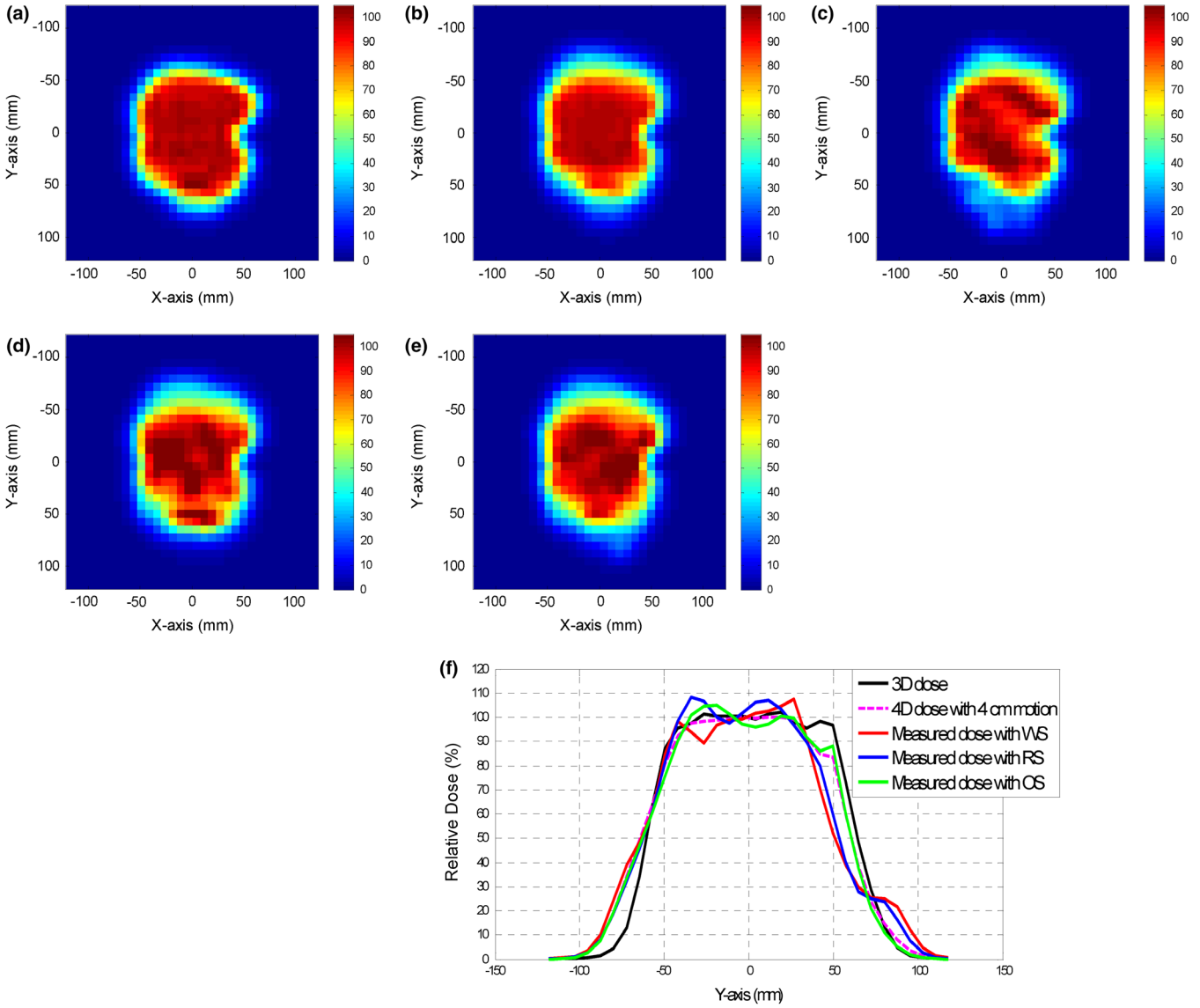

FIG. 8. Measurements of a patient field with heterogeneity using a wedge. (a) Nominal three-dimensional dose distribution. (b) Four-dimensional (4D) calculated dose distribution with 4-cm motion. (c) Single-fraction measured dose with worst delivery sequence (maximum dose error up to 25%). (d) Measurement for raster scanning delivery sequence (maximum dose error up to 15%). (e) Measurement for optimized delivery sequence (maximum dose error 8.6%). (f) Plot of y-axis with x = 0 for the nominal dose, 4D dose and measured doses with worst (WS), optimized (OS), and raster (RS) scanning sequences. Color bar represents relative dose.

deviations for each T'. Even under extreme motion conditions (e.g., 4-cm motion range and 10-s breathing cycle), the Poisson model predicted and bound the dose error. While the initial gain from increasing T' was quite drastic, the gain from increasing T' for each pencil beam diminished after $T' > 30$ s. Increasing T' from 30 to 50 s reduced the maximum dose error by only ~2.5%, as predicted by the Poisson model.

3.B. Patient treatment plan measurement results

Figure 8 shows the results for a patient plan measurement with a wedge and 4 cm of motion (maximum △WET of 4.8 cm) in a 10-s breathing period. The 4D dose was calculated by taking the average of the measured dose at the center of each phase, derived from the motion pattern; in other words, 10 measurements without motion were obtained to calculate the 4D dose. Figures 8(c) to 8(e) shows the measurement results with WS, RS, and OS, respectively. Figure 8(f) shows the plot of the y axis at $x = 0$ for the measurement results for the nominal, 4D, WS, OS, and RS sequences in a single fraction. The maximum dose error between the delivered dose and the 4D dose could be >50% for WS, >40% for RS, and ~10% for OS.

Figure 9 compares WS, RS, and OS for a patient treatment plan. Figure 9(a) shows T'_{mean} for each layer, with the WS, RS, and OS, from the highest energy to the lowest (155.3 to 86.4 MeV, total of 45). The WS, RS, and OS plans had a total delivery time of 238 s. Specifically,

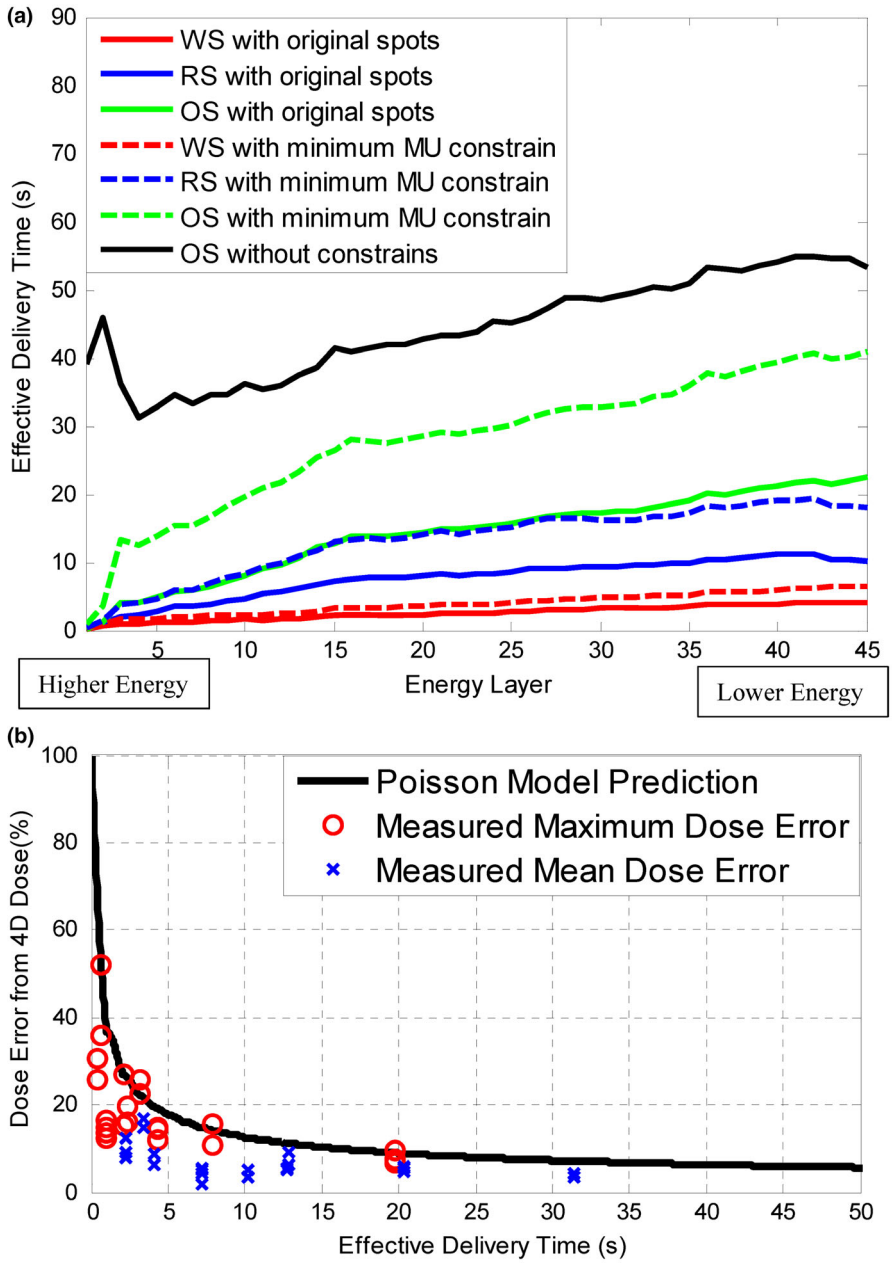

FIG. 9. Comparison of WS, RS, and OS in a patient plan. (a) Mean effective delivery time as a function of the energy layer for different spot sequence. The solid red (WS), blue (RS), and green (OS) lines have the same number of spots and a total delivery time of 238 s. Specifically, RS is the plan exported from the treatment planning system. The dashed red (WS), blue (RS), and green (OS) lines have the same number of spots and a total delivery time of 357 s. The black line does not satisfy delivery constraints, cannot be delivered by the PTC-H delivery system, and has a total delivery time of 1038 s. (b) The measured mean and maximum dose errors from the four-dimensional dose for patient treatment plan, with and without a wedge, as well as the theoretical upper bound with a Poisson model using Eq. (6).

RS is the plan exported from the treatment planning system. The delivery sequence was optimized using the methods presented above, with all delivery constraints considered, and resulted in an OS plan. The corresponding WS and RS plans were generated using the same number of spots and spot MUs. Therefore, the WS, RS, and OS plans had the same number of spots and a total delivery time of 357 s. An "ideal" plan without considering the delivery constraints was also generated and plotted; it did not satisfy the delivery constraints, cannot be delivered by the PTC-H delivery system, and had a total delivery time of 1038 s.

The 36 measurements of the deliverable plans are shown in Fig. 9(b). Again, the measured mean and maximum absolute dose errors from the 4D dose were plotted against the mean and minimum calculated effective delivery times, respectively. The Poisson upper bound based on Eq. (6) estimated the measurement results of a patient treatment plan, even with the most extreme motion condition: a 4-cm motion range, 10-s breathing cycle, and a 4.8-cm maximum $\triangle$WET.

With the OS plan, the measured maximum absolute dose error was 9.7%, and the mean absolute dose error was 3.3% in a single fraction.

4. DISCUSSION

Spot-scanning proton therapy can be highly sensitive to motion; we found that the motion-induced dose error was up to 100% in a single fraction if the delivery was not handled properly. The current study achieved its aim of quantifying dose uncertainty in a single fraction by developing an analytical model for the scanning beam delivery and patient breathing pattern. We found that the analytical model effectively estimated the upper bound of the dose error for a given treatment plan, even under extreme motion conditions. This method does not require repeated dose calculations and can easily incorporate techniques such as rescanning and spot delivery sequence optimization.[13,26]

A complete analytical model of patient breathing and the delivery system was built to calculate the upper bound of the motion-induced dose error from the 4D dose. It was established that the upper bound of the dose error is a function of the maximum dose error with $\triangle D^0_{\max}$ and T'. The $\triangle D^0_{\max}$ is, in turn, a function of motion amplitude (A), spot size (σ), and change in water equivalent thickness ($\triangle$WET); and T' is dependent on the spot delivery sequence, the timing parameters of the delivery system, and the breathing period (T_b). $\triangle D^0_{\max}$ is patient specific and can be conservatively set at 100%. T_b is patient specific and usually not a variable, and the timing parameters of the delivery system are fixed; therefore, the controlling factor of motion-induced dose uncertainty is the spot delivery sequence. Our study established that instead of actual delivery time,[8] the effective delivery time is associated with motion-induced dose uncertainties. The Poisson model–estimated dose error not only was validated by our extensive measurement, but also was consistent with previous studies at varies institutes on the relationship between dose error and delivery time/number of rescanning, even though the effective delivery time was not used in those studies.[11,30–33] Based on the analytical model of the PTC-H system, and 4D dynamic dose calculation evaluating the interplay effect,[15] we concluded that delivery sequence could have a great impact on the delivered dose to the patient when there were respiratory motion presented. We then proposed and studied a technique to optimize the delivery sequence in order to reduce the motion induce dose uncertainty. The delivery sequence optimization technique was applied to ten lung patients, and we showed that the optimized delivery sequence developed based on the analytical model reduces the mean of fractional maximum absolute dose error compared with the regular delivery sequence by 3.3% to 10.6% (32.5%–68.0% relative reduction) for different patients.[26] While the patient number was limited, these results further validated the analytical model for lung patients.

The current study used the delivery parameters for PTC-H, but the principle of the model remains the same for all spot-scanning proton delivery machines and could be easily customized for different delivery systems. In particular, in this study we assumed a monotonically decreasing energy during delivery owing to current system constraints. However, with advanced energy switching techniques such as multiple energy extraction,[34] the order of energy delivery could be optimized in addition to the spot delivery sequence, which possibly lead to a deliverable plan for patient treatment even with large tumor motion [Fig. 9(a)]. We also only modeled the proton spot using a single Gaussian model. However, since the second Gaussian used in the double Gaussian model of the proton spots[35] has a large σ and low weighting, it contributes little to the motion-induced uncertainty, as established in this study.

Our study assumed the scanning beam proton delivery and patient breathing are completely independent, and that patient breathing was not monitored or regulated during treatment. However, if patient breathing pattern were monitored and proton beam delivery could be correlated to patient breathing, motion mitigation could be achieved more efficiently, in that one could now "assign" the spots to be delivered to a certain phase, instead of counting on the spots to "arrive" at those phases. Investigation on fast beam delivery with patient motion monitor has been conducted by several groups[36–38] but is outside the scope of the current study. Another limitation of the study is that we assumed the patient′s position and breathing pattern remained the same as that of the 4DCT throughout treatment. This assumption was inherited from the treatment planning process and may not be valid in practice. Therefore, clinically, it is important to monitor patients′ position and breathing during treatment and provide training as needed. The dose deviation from the 4D dose with breathing pattern irregularity would be a function of the fractional time of patient breathing amplitude of the 4DCT range; while conceptually, the optimized dose delivery sequence would minimize this dose deviation as well,[39] quantitative evaluation in a patient setting is necessary. For patient positioning and range uncertainties, the incorporation of robust optimization might mitigate the problem but further evaluation is necessary.

5. CONCLUSIONS

After extensive validation, we conclude that our analytical model effectively estimates the upper bound of dose uncertainty for spot-scanning proton therapy.

ACKNOWLEDGMENTS

The authors would like to thank Sarah Bronson of MD Anderson's Scientific Publications Department for her suggestions for and careful review of this manuscript.

[a]Author to whom correspondence should be addressed. Electronic mail: hengli@jhu.edu.

REFERENCES

1. Zhang X, Li Y, Pan X, et al. Intensity-modulated proton therapy reduces the dose to normal tissue compared with intensity-modulated radiation therapy or passive scattering proton therapy and enables individualized radical radiotherapy for extensive stage IIIB non-small-cell lung cancer: a virtual clinical study. *Int J Radiat Oncol Biol Phys*. 2010;77:357–366.
2. Chang JY, Li H, Zhu XR, et al. Clinical implementation of intensity modulated proton therapy for thoracic malignancies. *Int J Radiat Oncol Biol Phys*. 2014;90:809–818.
3. Engelsman M, Schwarz M, Dong L. Physics controversies in proton therapy. *Sem Radiat Oncol*. 2013;23:88–96.
4. Phillips MH, Pedroni E, Blattmann H, Boehringer T, Coray A, Scheib S. Effects of respiratory motion on dose uniformity with a charged particle scanning method. *Phys Med Biol*. 1992;37:223–234.
5. Bert C, Durante M. Motion in radiotherapy: particle therapy. *Phys Med Biol*. 2011;56:R113–R144.
6. Lambert J, Suchowerska N, McKenzie DR, Jackson M. Intrafractional motion during proton beam scanning. *Phys Med Biol*. 2005;50:4853–4862.
7. Bert C, Grozinger SO, Rietzel E. Quantification of interplay effects of scanned particle beams and moving targets. *Phys Med Biol*. 2008;53:2253–2265.
8. Dowdell S, Grassberger C, Sharp GC, Paganetti H. Interplay effects in proton scanning for lung: a 4D Monte Carlo study assessing the impact of tumor and beam delivery parameters. *Phys Med Biol*. 2013;58:4137–4156.
9. Grassberger C, Dowdell S, Lomax A, et al. Motion interplay as a function of patient parameters and spot size in spot scanning proton therapy for lung cancer. *Int J Radiat Oncol Biol Phys*. 2013;86:380–386.
10. Kraus KM, Heath E, Oelfke U. Dosimetric consequences of tumour motion due to respiration for a scanned proton beam. *Phys Med Biol*. 2011;56:6563–6581.
11. Seco J, Robertson D, Trofimov A, Paganetti H. Breathing interplay effects during proton beam scanning: simulation and statistical analysis. *Phys Med Biol*. 2009;54:N283–N294.
12. Engwall E, Glimelius L, Hynning E. Effectiveness of different rescanning techniques for scanned proton radiotherapy in lung cancer patients. *Phys Med Biol*. 2018;63:095006.
13. Chang JY, Zhang X, Knopf A, et al. Consensus guidelines for implementing pencil-beam scanning proton therapy for thoracic malignancies on behalf of the PTCOG thoracic and lymphoma subcommittee. *Int J Radiat Oncol Biol Phys*. 2017;99:41–50.
14. Jakobi A, Perrin R, Knopf A, Richter C. Feasibility of proton pencil beam scanning treatment of free-breathing lung cancer patients. *Acta Oncol*. 2018;57:203–210.
15. Kardar L, Li Y, Li X, et al. Evaluation and mitigation of the interplay effects of intensity modulated proton therapy for lung cancer in a clinical setting. *Pract Radiat Oncol*. 2014;4:e259–e268.
16. Li Y, Kardar L, Li X, et al. On the interplay effects with proton scanning beams in stage III lung cancer. *Med Phys*. 2014;41:021721.
17. Gillin MT, Sahoo N, Bues M, et al. Commissioning of the discrete spot scanning proton beam delivery system at the University of Texas M.D. Anderson Cancer Center, Proton Therapy Center, Houston. *Med Phys*. 2010;37:154–163.
18. Li Y, Zhu RX, Sahoo N, Anand A, Zhang X. Beyond Gaussians: a study of single-spot modeling for scanning proton dose calculation. *Phys Med Biol*. 2012;57:983–997.
19. Zhu XR, Poenisch F, Lii M, et al. Commissioning dose computation models for spot scanning proton beams in water for a commercially available treatment planning system. *Med Phys*. 2013;40:041723.
20. Zhu XR, Sahoo N, Zhang X, et al. Intensity modulated proton therapy treatment planning using single-field optimization: the impact of monitor unit constraints on plan quality. *Med Phys*. 2010;37:1210–1219.
21. Li H, Li Y, Zhang X, et al. Dynamically accumulated dose and 4D accumulated dose for moving tumors. *Med Phys*. 2012;39:7359–7367.
22. Court L, Wagar M, Bogdanov M, et al. Use of reduced dose rate when treating moving tumors using dynamic IMRT. *J Appl Clin Med Phys*. 2011;12:3276.
23. Furukawa T, Inaniwa T, Sato S, et al. Design study of a raster scanning system for moving target irradiation in heavy-ion radiotherapy. *Med Phys*. 2007;34:1085–1097.
24. Furukawa T, Inaniwa T, Sato S, et al. Moving target irradiation with fast rescanning and gating in particle therapy. *Med Phys*. 2010;37:4874–4879.
25. Mori S, Inaniwa T, Furukawa T, et al. Amplitude-based gated phase-controlled rescanning in carbon-ion scanning beam treatment planning under irregular breathing conditions using lung and liver 4DCTs. *J Radiat Res*. 2014;55:948–958.
26. Li H, Zhu XR, Zhang X. Reducing dose uncertainty for spot-scanning proton beam therapy of moving tumors by optimizing the spot delivery sequence. *Int J Radiat Oncol Biol Phys*. 2015;93:547–556.
27. George R, Vedam SS, Chung TD, Ramakrishnan V, Keall PJ. The application of the sinusoidal model to lung cancer patient respiratory motion. *Med Phys*. 2005;32:2850–2861.
28. Lujan AE, Larsen EW, Balter JM, Ten Haken RK. A method for incorporating organ motion due to breathing into 3D dose calculations. *Med Phys*. 1999;26:715–720.
29. Fitzpatrick MJ, Starkschall G, Balter P, et al. A novel platform simulating irregular motion to enhance assessment of respiration-correlated radiation therapy procedures. *J Appl Clin Med Phys*. 2005;6:13–21.
30. Grassberger C, Dowdell S, Sharp G, Paganetti H. Motion mitigation for lung cancer patients treated with active scanning proton therapy. *Med Phys*. 2015;42:2462–2469.
31. Bernatowicz K, Lomax AJ, Knopf A. Comparative study of layered and volumetric rescanning for different scanning speeds of proton beam in liver patients. *Phys Med Biol*. 2013;58:7905–7920.
32. Knopf AC, Hong TS, Lomax A. Scanned proton radiotherapy for mobile targets-the effectiveness of re-scanning in the context of different treatment planning approaches and for different motion characteristics. *Phys Med Biol*. 2011;56:7257–7271.
33. Zenklusen SM, Pedroni E, Meer D. A study on repainting strategies for treating moderately moving targets with proton pencil beam scanning at the new Gantry 2 at PSI. *Phys Med Biol*. 2010;55:5103–5121.
34. Younkin JE, Bues M, Sio TT, et al. Multiple energy extraction reduces beam delivery time for a synchrotron-based proton spot-scanning system. *Adv Radiat Oncol*. 2018;3:412–420.
35. Sawakuchi GO, Titt U, Mirkovic D, et al. Monte Carlo investigation of the low-dose envelope from scanned proton pencil beams. *Phys Med Biol*. 2010;55:711–721.
36. Mori S, Karube M, Shirai T, et al. Carbon-ion pencil beam scanning treatment with gated markerless tumor tracking: an analysis of positional accuracy. *Int J Radiat Oncol Biol Phys*. 2016;95:258–266.
37. Ebner DK, Tsuji H, Yasuda S, Yamamoto N, Mori S, Kamada T. Respiration-gated fast-rescanning carbon-ion radiotherapy. *Jpn J Clin Oncol*. 2017;47:80–83.
38. Poulsen PR, Eley J, Langner U, Simone CB 2nd, Langen K. Efficient interplay effect mitigation for proton pencil beam scanning by spot-adapted layered repainting evenly spread out over the full breathing cycle. *Int J Radiat Oncol Biol Phys*. 2018;100:226–234.
39. Koybasi O, Mishra P, St James S, Lewis JH, Seco J. Simulation of dosimetric consequences of 4D-CT-based motion margin estimation for proton radiotherapy using patient tumor motion data. *Phys Med Biol*. 2014;59:853–867.